Preparation and *in vitro* characterization of novel bioactive glass ceramic nanoparticles

Zhongkui Hong,[1,2] Rui L. Reis,[1,2] João F. Mano[1,2]
[1]*3B's Research Group – Biomaterials, Biodegradables and Biomimetics, Department of Polymer Engineering, University of Minho, Campus de Gualtar, 4710-057 Braga, Portugal*
[2]*IBB – Institute for Biotechnology and Bioengineering, Braga, Portugal*

Received 3 September 2007; revised 5 October 2007; accepted 18 October 2007
Published online 19 February 2008 in Wiley InterScience (www.interscience.wiley.com). DOI: 10.1002/jbm.a.31848

Abstract: SiO_2-CaO-P_2O_5 ternary bioactive glass ceramic (BGC) nanoparticles with different compositions were prepared via a three-step sol-gel method. Polyethylene glycol was selected to be used as the surfactant to improve the dispersion of the nanoparticles. The morphology and composition of these BGC nanoparticles were observed by ESEM and EDX. All the BGC particles obtained in this method were about 20 nm in diameter. XRD analysis demonstrated that the different compositions can result in very different crystallinities for the BGC nanoparticles. Bioactivity tests in simulated body fluid solution (SBF), and degradability in phosphate buffer solution (PBS), were performed *in vitro*. SEM, EDX, and XRD were employed to monitor the surface variation of neat poly(L-lactic acid), PLLA, foam and PLLA/BGC porous scaffolds during incubation. The BGC nanoparticles with lower phosphorous and relative higher silicon content exhibited enhanced mineralization capability in SBF and a higher solubility in PBS medium. Such novel nanoparticles may have potential to be used in different biomedical applications, including tissue engineering or the orthopedic field. © 2008 Wiley Periodicals, Inc. J Biomed Mater Res 88A: 304–313, 2009

Key words: nanoparticles; apatite; glass ceramic; nanocomposites; bone tissue engineering

INTRODUCTION

Since Hench et al.[1] developed the Bioglass®, increasing attention has been paid to bioactive glasses and glass-ceramic systems for their excellent biocompatibility and bioactivity in bone tissue engineering. It has been found that silicon component plays the key role in bone mineralization instead of calcium. When implanted, bioactive glass can release soluble silicon via interfacial reaction with body fluid and induces the formation of calcium deficient hydroxyapatite (HAP) layer on the surface of bioactive glass. This biologically active HAP layer is chemically similar with the mineral phase of natural bone, allowing bioactive glass to chemically bond to surrounding tissue. So, the formation of HAP is the critical stage for the bonding of bioactive glasses to regenerated bone and to promote the contact between the implant and the host bone tissue.[2] *In vivo* studies showed that bioactive glass system has remarkable advantage for regeneration of bone tissue compared to HAP ceramic.[3] It is generally accepted that bioactive glass is a more promising biomaterial than HAP in bone tissue engineering.[4–6]

Numerous reports about preparation of bioactive glass materials have been published in past decades, including bulk bioactive glass,[7–10] bioactive glass particles, and their composites.[11–22] The structure and composition of the glasses can be tailored by controlling the fabrication parameter.[23,24] Different types of bioactive glasses were designed for different utilization in bone tissue engineering. Porous bioactive glass can be obtained by sol–gel methods based on the use of granular polyethylene glycol (PEG) as pore former. Its porous structure, with coexistent macro and mesopores, was suitable for tissues and blood vessel ingrowths, and presented simultaneously the capability of forming a HAP surface layer.[7] Such advantages make these bioactive glass promising materials to be used in bone tissue engineering and bone regeneration.

However, compared with natural bone tissue, bioactive glasses, especially when processed as foams,

Correspondence to: J. F. Mano; e-mail: jmano@dep.uminho.pt

Contract grant sponsor: FCT; contract grant numbers: POCTI/FIS/61621/2004, SFRH/BPD/25828/2005, PTDC/QUI/69263/2006

exhibit lower mechanical properties. In particular, the low fracture toughness limits the application of bioactive glasses as scaffold structures in load-bearing situations. General values of mechanical properties for bulk bioactive glass materials were summarized by Rezwan et al.[25]

The development of biopolymer/bioactive glass and biopolymer/bioactive ceramic composites has been recognized as a strategy to improve the mechanical behavior of bioactive glass-based materials.[11–14] Composites combining bioactive glass particles and biopolymers have become very promising systems for bone reconstruction or regeneration by combining the advantages of each component in one material.[15–22] Compared with microsized bioactive ceramic particles, nanosized particles have a large surface area and can form a more tight interface with polymer matrix in composites, and hence, a high performance in mechanical properties can be expected.[26–29] In this context, most of the studies have been reporting systems based on HAP nanoparticles and the works based on bioactive glasses are scarce.[30–33] In this work, bioactive glass ceramic (BGC) nanoparticles with different compositions were prepared by means of a three-step sol–gel method, and the physical, chemical, and bioactive properties of these nanoparticles were characterized. To check the bioactive character in potential tissue engineering applications, model scaffolds were prepared by combining poly(L-lactic acid), and the produced glass ceramic nanoparticles.

MATERIALS AND METHODS

Materials

Tetraethoxysilane (TEOS), calcium nitrate, citric acid, and ammonium dibasic phosphate were obtained from Sigma. PEG (M_n: 16,000–24,000) and Dioxane were purchased from Fluka. Poly(L-lactic acid) (PLLA, M_w: 200,000) was obtained from Stratec.

Preparation of BGC nanoparticles based on SiO_2-CaO-P_2O_5

The procedure for preparing the BGC-55 nanoparticles (SiO_2:CaO:P_2O_5 (mol) = 55:40:5) was based on the method reported elsewhere[34] and was described as follows: (1) In an well-washed beaker equipped with a magnetic stirrer, 7.639 g calcium nitrate was dissolved in 120 mL of deionized water at room temperature. The TEOS-ethanol solution was created by diluting 9.167 g of TEOS in 60 mL of ethanol and added to the calcium nitrate solution. Then, citric acid was added into the solution to adjust the pH value to 1–2. The reaction mixture was kept stirring until a homogeneous and transparent solution was obtained. (2) Under vigorous stirring, the homogenous solution was slowly dropped into 1500 mL of ammoniated deionized water, in which 1.078 g of ammonium dibasic phosphate was dissolved in advance. During the dripping process the pH value of solution was kept at around 11 using ammonia water. (3) After stirred 48 h and aged for 24 h, the precipitate was separated from the reaction solution by centrifugation at 1000 rpm, washed three times with deionized water, and finally separated in 200 mL of 2% PEG-water solution and kept still. (4) The precipitation was freeze dried and followed by calcination at 700°C in a muffle furnace for 3 h, after which the white BGC nanoparticles were obtained. BGC-30 (SiO_2 : CaO : P_2O_5 (mol) = 30 : 60 : 10) and BGC-68 (SiO_2 : CaO : P_2O_5 (mol) = 68 : 28 : 4) were also obtained in this route by variation of reactant quantity.

Preparation of PLLA/BGC nanocomposite scaffold

Preparation of PLLA/BGC composite porous scaffolds was based on thermal induced phase separation that was similar with the process described elsewhere.[35] Briefly, a given amount of BGC powder was homogeneously suspended in dioxane with ultrasonication and magnetic stir. PLLA was dissolved in a BGC-dioxane suspension to produce a polymer weight to solvent volume ratio of 5%. The mixture was stirred overnight to obtain a homogeneous polymer solution. After lyophilization at −80°C for 1 week, porous PLLA/BGC composite scaffolds were obtained.

Field emission scanning electron microscopy

The morphology of the BGC nanoparticles was observed using field emission scanning electron microscopy (ESEM) (XL30 ESEM FEG; Philips) equipped with energy-dispersive X-ray spectroscopy (EDX).

Fourier-transformed infrared spectroscopy analysis

A Bio-Rad Win-IR spectrometer was employed for the Fourier-transformed infrared (FTIR) spectroscopy analysis. The samples of BGC powders were mixed with KBr powder and pressed into a disk suitable for FTIR measurement. The FTIR spectra were recorded from 4000 cm^{-1} to 400 cm^{-1}.

X-ray diffraction

X-ray diffraction (XRD) analysis were performed on an X-ray diffractometer (Philips PW 1710, Netherlands) with a Cu Kα radiation (λ = 0.154 nm). Voltage and current were selected at 40 kV and 50 mA, respectively. Data were collected from 2θ = 10° to 60° with a step size of 0.02°.

In vitro bioactivity study

In vitro bioactivity test were carried out by soaking the 10 × 10 × 2 mm^3 porous scaffolds in 10 mL of simulated body fluid (SBF) (Na^+ 142.0, K^+ 5.0, Ca^{2+} 2.5, Mg^{2+} 1.5, Cl^-

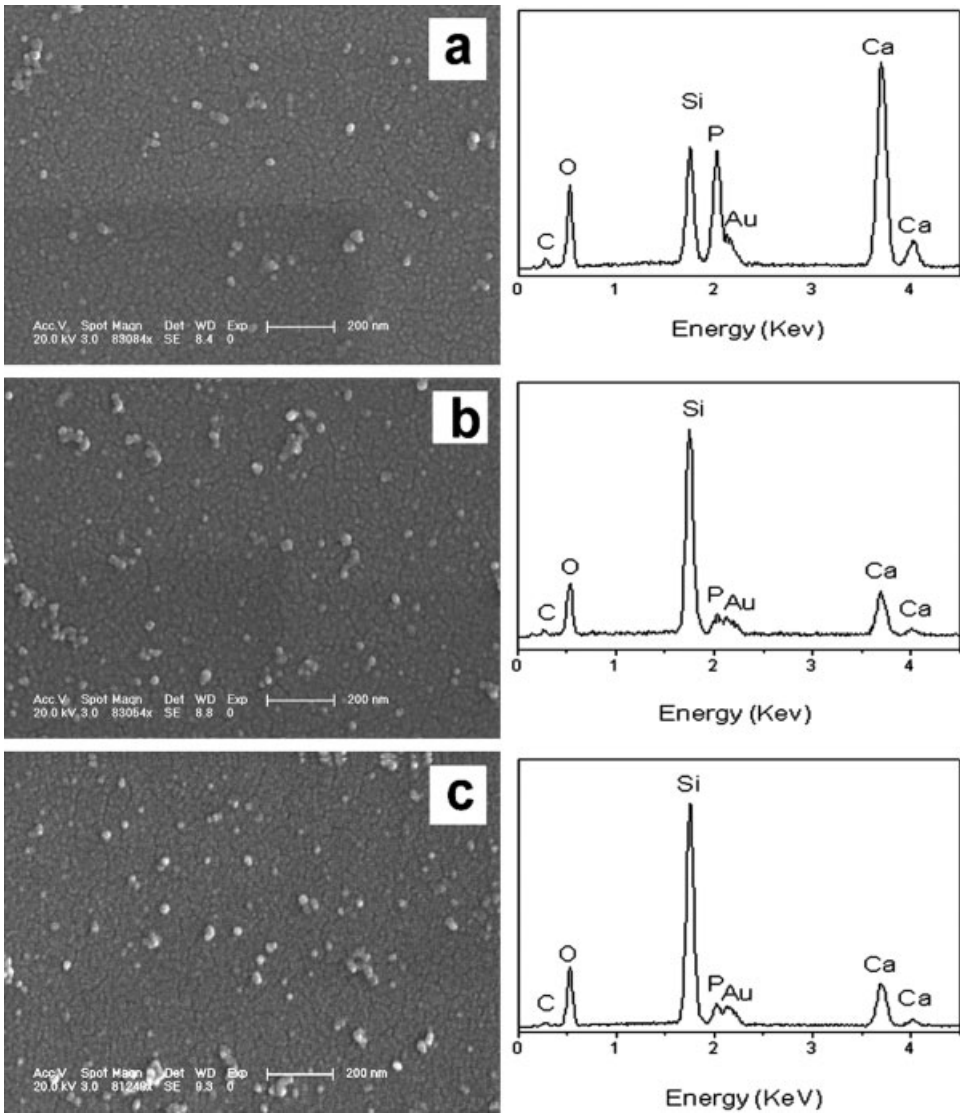

Figure 1. ESEM micrographs and EDX curves for BGC nanoparticles with different compositions. (a) BGC-30, (b) BGC-55, and (c) BGC-68. Bar is 200 nm.

148.0, HCO^{3-} 4.2, HPO_4^{2-} 1.0, SO_4^{2-} 0.5 m*M*) in conical flasks, and placed in an oven at 37°C for periods of 1, 3, 7, 14, and 21 days. To terminate the reactions after the different soaking periods, the scaffolds were taken out from SBF, rinsed with deionized water, and freeze dried for 1 week. The formation of apatite onto the porous PLLA and PLLA/BGC composite were characterized by SEM, EDX, and XRD. For SEM observation, samples were coated with gold. For EDX analysis, all samples were coated with carbon to avoid the overlap of the peaks of gold and phosphorous.[14,36]

SEM and EDX analysis

The morphologies of the PLLA and PLLA/BGC composites after soaking in SBF for different periods were observed using SEM (Leica Cambridge S 360 microscope). For SEM observation, samples were coated with gold. For EDX analysis, all samples were coated with carbon to avoid the overlap of the peaks of gold and phosphorous.

In vitro degradation study

For degradation experiments, samples of neat polymer and composite scaffolds were cut into small pieces with dimensions of 10 × 10 × 2 mm^3. The samples were sterilized by UV exposure under a laminar flow hood for 10 min on each side and placed in sterile Falcon tube. For each time point, three samples of each scaffold composition were immersed in 10 mL of phosphate-buffered saline. The phosphate buffer solution (PBS) was prepared by dissolving one tablet of PBS, from Sigma-Aldrich, in 200 mL of distilled water to obtain a final concentration of 0.227*M* potassium chloride and 0.137*M* sodium chloride, at pH = 7.4. The samples were incubated under slow tangential agitation at 37°C. The pH of the buffer was monitored

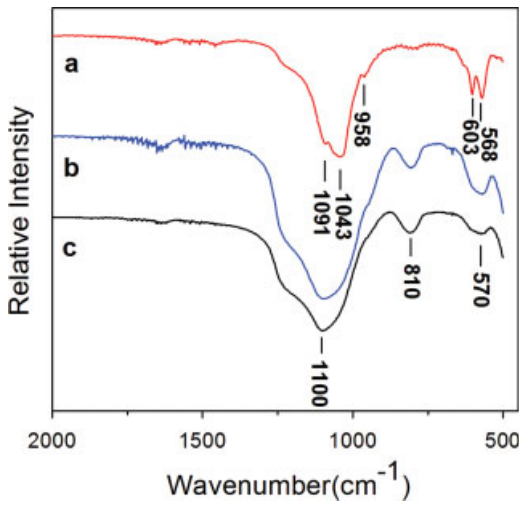

Figure 2. FTIR spectra of BGC nanoparticles with different compositions. (a) BGC-30, (b) BGC-55, and (c) BGC-68. [Color figure can be viewed in the online issue, which is available at www.interscience.wiley.com.]

during the experiment. At different time points, samples of each scaffold composition were removed from the PBS and weighted (W_w) after surface wiping with filter paper. Each sample was drastically rinsed with deionized water to remove the soluble inorganic salt, and weighed (W_d) after completely dried in oven. The pH of the medium was recorded at each time point. Water absorption (W_A%) and weight loss (W_L%) were calculated according to Eqs. (1) and (2), respectively:

$$W_A\% = [(W_w - W_i)/W_i] \times 100\% \quad (1)$$

$$W_L\% = [(W_d - W_i)/W_i] \times 100\% \quad (2)$$

where W_i was the initial weight of each sample.

RESULTS AND DISCUSSION

BGC nanoparticles

ESEM micrographs and EDX curves of BGC particles with different compositions are shown in Figure 1. Most of BGC particles exhibit a spherical form with about 20 nm in diameter. No obvious difference both in size and morphology could be seen between the three sets of samples. EDX curves showed the different concentrations of Si, P, and Ca, which well agreed with the different compositions of three types of the BGC nanoparticles studied.

The FTIR spectra of the BGC nanoparticles with different compositions were presented in Figure 2. Two peaks at 1043 and 1091 [Fig. 2(a)] arose from P—O bond were shifted to a broad and strong absorption band at 1100 cm^{-1} [Fig. 2(b,c)] that could be ascribed to the stretch vibration of Si—O—Si bond. Small band at 810 cm^{-1} was the absorption band of symmetric stretch vibration of Si—O bond. Two sharp bands could also be noted at 603 cm^{-1} and 568 cm^{-1} in Figure 1(a), which should be attributed to the bending vibration of P—O bond in crystal phosphate. These twin bands merged into a weak dispersive band at 570 cm^{-1} in Figure 1(a), which arose from the bending vibration of amorphous P—O bond.

Figure 3 showed the XRD spectra of the BGC powders with the different compositions. The spectra of BGC-55 and BGC-68 were a broad dispersive band as shown in Figure 3(b,c), indicating the amorphous nature of the two materials. BGC-30 was crystalline, showing sharp phosphate crystal peaks appeared at $2\theta = 32^\circ$ and $2\theta = 26^\circ$ [see Fig. 3(a)]. Such results shows that the crystallinity of BGC particles obtained at the same preparation condition could increase with increasing phosphate content, being in agreement with the FTIR results.

In vitro bioactivity tests

The morphology of the porous scaffolds of PLLA and the composite of PLLA/25% BGC-30 was shown in Figure 4. SEM images of neat PLLA foam [Fig. 4(a,b)] showed a continuous microstructure of nearly interconnected pores with dimensions between 10 and 300 μm diameter. The morphology of PLLA/BGC foam did not show too much difference from the image of the PLLA scaffold. This was an indication that the BGC particles did not remarkably change the mechanism of pore formation by crystallization of dioxane solvent at 25 wt % of BGC load. In the high magnification image of PLLA/BGC composite [Fig. 4(d)], some microsized BGC clusters could be seen on the wall of microporous structure,

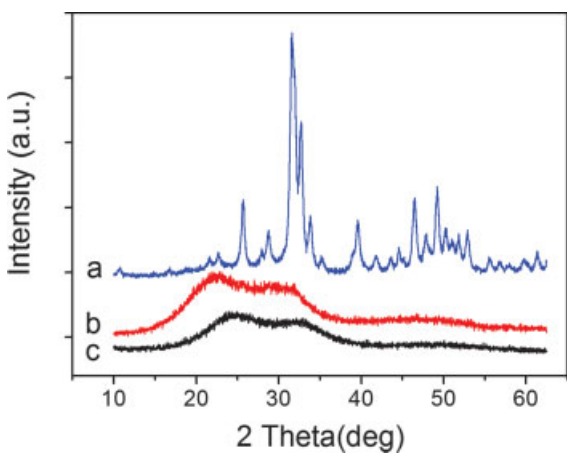

Figure 3. XRD patterns for the BGC nanoparticles with different compositions. (a) BGC-30, (b) BGC-55, and (c) BGC-68. [Color figure can be viewed in the online issue, which is available at www.interscience.wiley.com.]

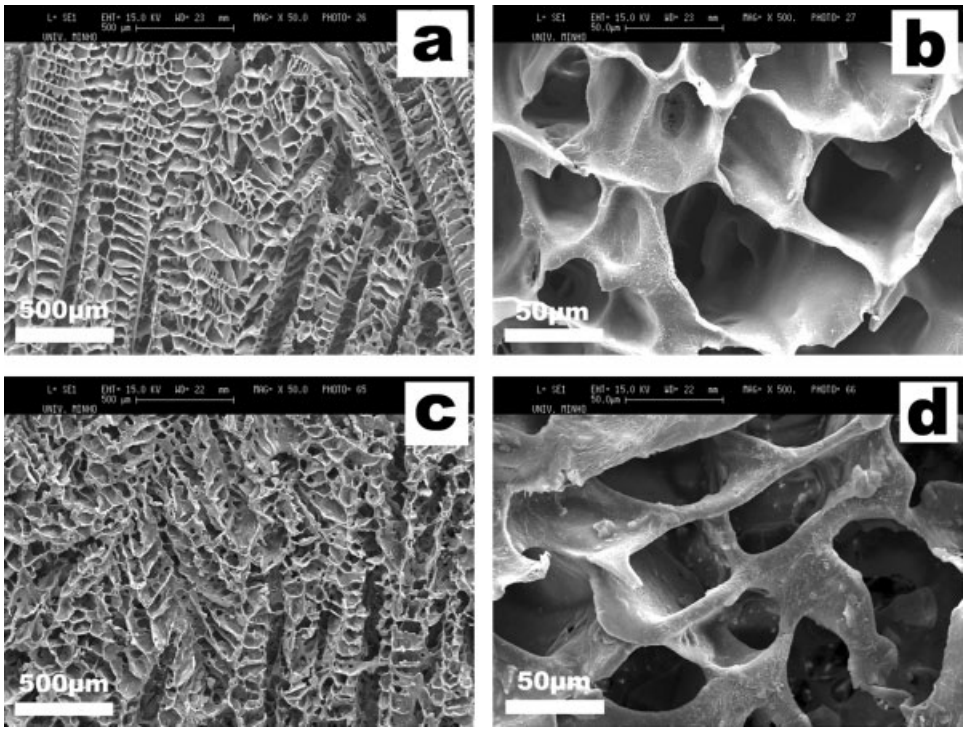

Figure 4. SEM micrographs for the PLLA scaffold at (a) low magnification and (b) high magnification. The morphology of the PLLA/BGC-30 composite scaffold is also shown at (c) low magnification and (d) high magnification.

which revealed that BGC particles can, to some extent, agglomerate in the PLLA matrix at 25 wt % of BGC content.

Figure 5 shows the morphology of porous PLLA and PLLA/BGC composites scaffolds after soaking in SBF for different periods. Different types of BGC particles exhibit very different bioactive performance in SBF. After 1 day of immersion in SBF, the cauliflower-like apatite cluster formed on the surface of PLLA/BGC-55 and PLLA/BGC-68 composites as shown in Figure 5(c_1,d_1), and grew with increasing immersion time as shown in Figure 5(c_3,d_3). After 14 days of incubation, most of the PLLA/BGC-55 and PLLA/BGC-68 scaffold surfaces were covered by needle-like apatite layer as shown in Figure 5(c_{14},d_{14}). The apatite layers were further thickened in the SEM images after 21 days of incubation period [Fig. 5(c_{21},d_{21})]. Oppositely, no apatite formation was detected in the SEM images for both neat PLLA and PLLA/BGC-30 composite after soaking in SBF for different times [see Fig. 5(a,b)].

The results obtained by SEM were confirmed by EDX analysis (see Fig. 6). No notorious changes could be detected in the EDX curves for PLLA and PLLA/BGC-30 composite before and after soaking in SBF [Fig. 6(a,b)], whereas a significant variation in the intensity of Si, P, and Ca can be observed on Figure 6(c,d). It could be noticed that after soaking in SBF, the concentrations of Ca and P gradually and significantly increased accompanied by the decreasing of concentration of Si, in comparison with the initial materials, which strengthens the indication of a development of apatite material onto the surfaces of PLLA/BGC-55 and PLLA/BGC-68.[14,37] FTIR analysis has proved that this apatite formed by inducement of BGC nanoparticles in SBF was carbonated hydroxyapatite particles.[34]

To characterize the inorganic phase formed onto the surfaces of PLLA/BGC-55 and PLLA/BGC-68 scaffolds, XRD analysis was performed on the different materials. Figure 7 shows XRD patterns of the PLLA and the different PLLA/BGC nanocomposites after soaking in SBF for 14 days. As observed in Figure 7(a), porous PLLA scaffold displays a typical amorphous behavior, which indicated that the crystallization of PLLA could be prevented by the processing technique utilized. In Figure 7(c,d), the typical crystalline diffraction pattern of apatite can be observed with an evident peak at $2\theta = 31.7^\circ$, which confirms that partially crystallized apatite layer formed on the surfaces of PLLA/BGC-55 and PLLA/BGC-68. For PLLA/BGC-30 composite [Fig. 7(b)], an obvious peak appeared near $2\theta = 32.4^\circ$. However, it was not clear of the origin of the peaks because there was overlapping between the peaks of the BGC-30 nanoparticles and apatite that may form on the surface of PLLA/BG-30 composite after soaking in SBF.

In summary, BGC-55 and BGC-68 exhibit more pronounced bioactivity behavior, as tested *in vitro* using SBF, than BGC-30. This finding was in agreement

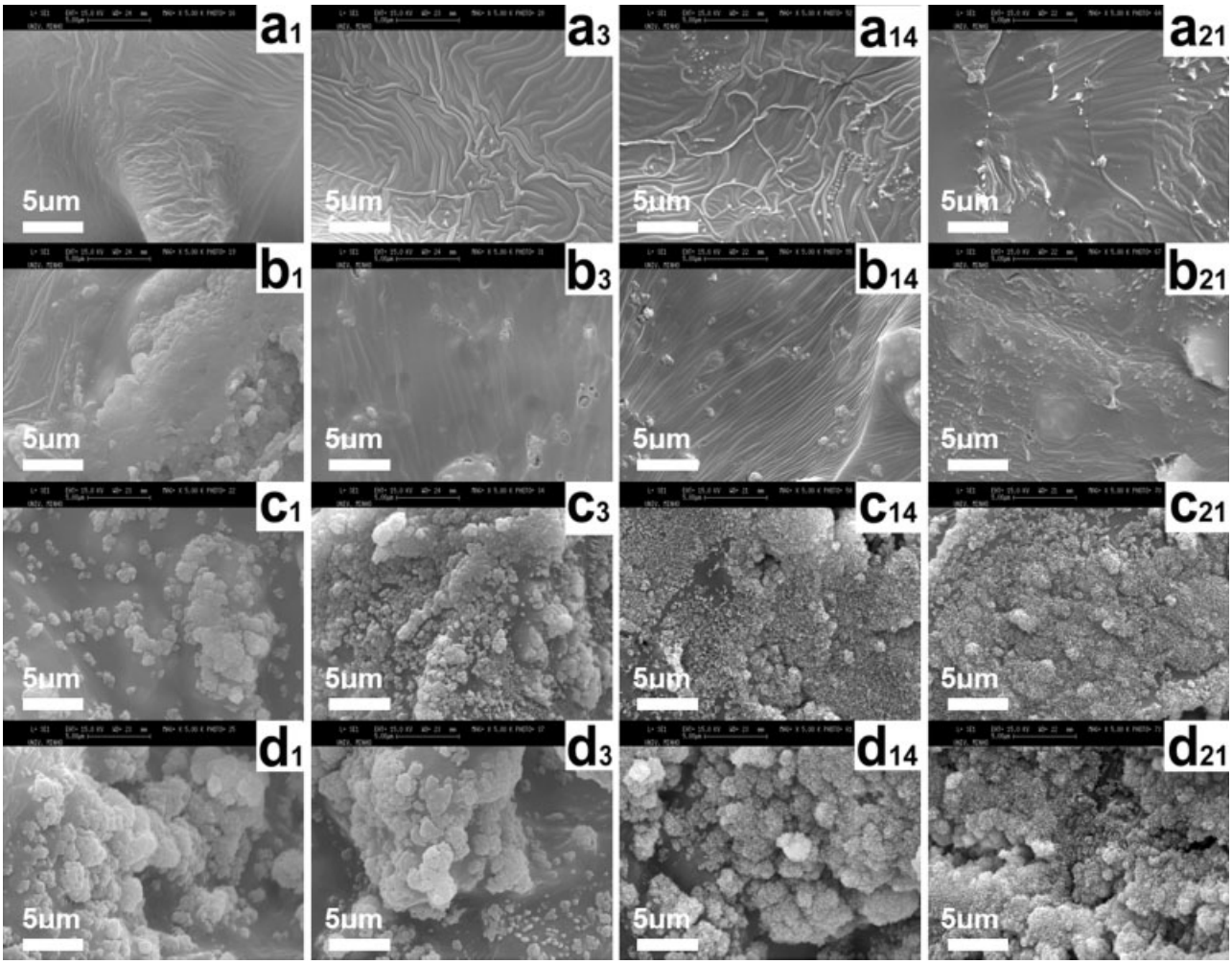

Figure 5. SEM micrographs for the PLLA scaffold (a) and the different types of PLLA/BGC composites after incubation in SBF for different periods: (b) BGC-30, (c) BGC-55, and (d) BGC-68. The subscripts indicate the different incubation times in SBF (in days).

with previous report that crystallization of bioactive glasses decreases the level of bioactivity and even turns a bioactive glass into bioinert material. The formation of a crystalline apatite layer on the surface of BGC materials was a very complicated process. Several steps of chemical and physical reaction such as solubility of BGC material, ion exchange between BGC and SBF solution, and hydroxylation of the materials surface were involved in this biomimetic process. The amorphous phase of BGC controlled the rate of ion exchange and silanol formation; the less crystallized BGC materials demonstrated higher bioactivity in mineralization test *in vitro*.[38,39]

In vitro degradation of nanocomposite of PLLA and BGC

To study the solubility of different types of BGC and their effect on the degradation behavior of PLLA matrix, the *in vitro* degradation profile of PLLA and composite samples were determined as a function of the incubation time in PBS (pH = 7.4) at 37°C. The degradation of PLLA and PLLA/BGC composites was monitored by water absorption, weight loss, and pH variation in PBS medium.

Figure 8 showed the water absorption of neat PLLA and PLLA/BGC composites foams. It was observed that after 1 day of immersion in PBS, all samples exhibit considerable water uptake values due mostly to the filling of the pores with water. There was a mass increase of 600% for pure PLLA foam, whereas for all PLLA/BGC composites water uptake was about 650%. Comparing with PLLA porous scaffold, the water absorption rate should have a remarkable increase for PLLA/BGC composite with the introduction of hydrophilic BGC powder.[35] However, no obvious increase in water absorption rate could be seen between the PLLA and PLLA/BGC composites, which should be due to the

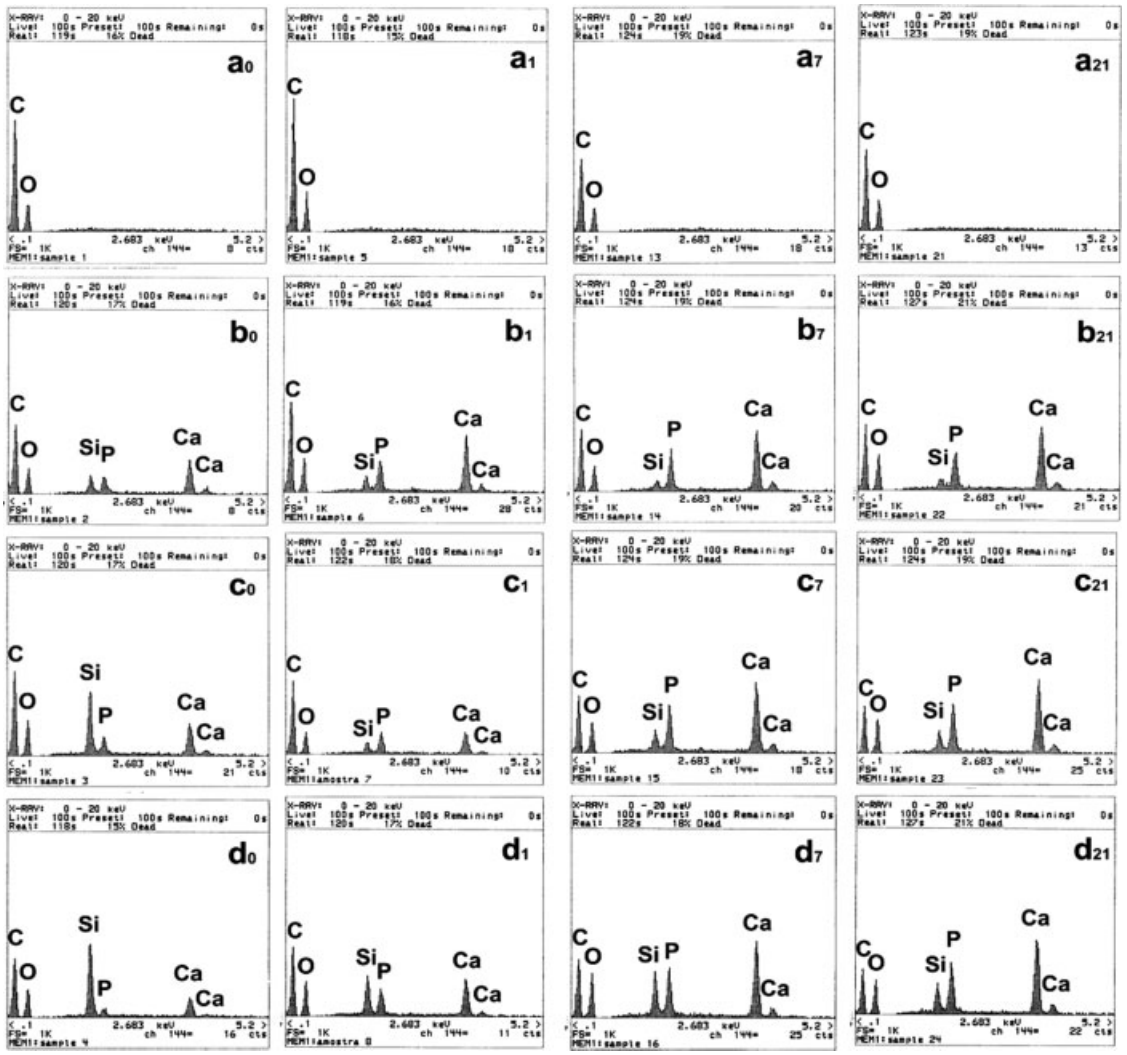

Figure 6. EDX curves for the PLLA scaffold (a) and the different types of PLLA/BGC composites after incubation in SBF for different periods: (b) BGC-30, (c) BGC-55, and (d) BGC-68. The subscripts indicate the different incubation times in SBF (in days).

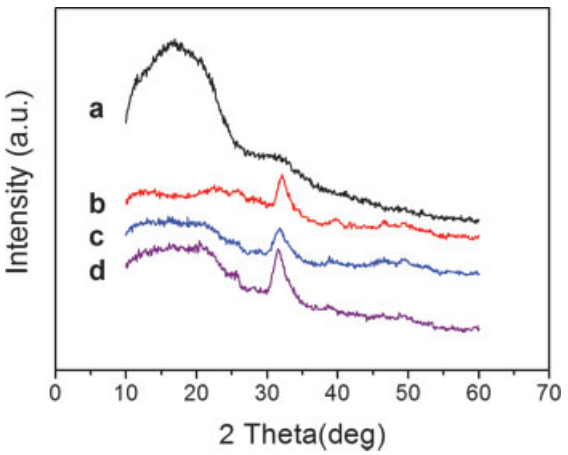

Figure 7. XRD patterns for the PLLA scaffold (a) and the different types of PLLA/BGC composites after incubation in SBF for 14 days: (b) BGC-30, (c) BGC-55, and (d) BGC-68. [Color figure can be viewed in the online issue, which is available at www.interscience.wiley.com.]

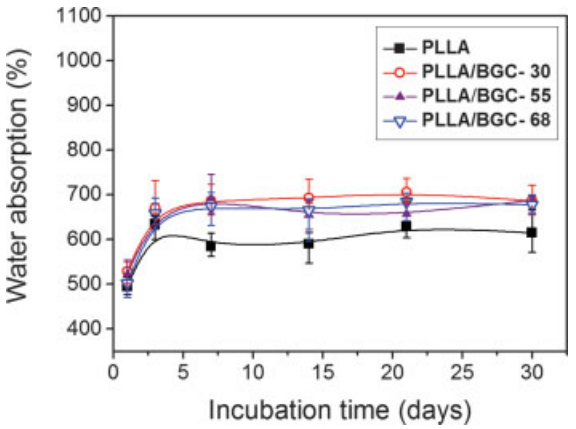

Figure 8. Water absorption versus incubation time in PBS for the porous scaffold of PLLA and the different types of PLLA/BGC composites. [Color figure can be viewed in the online issue, which is available at www.interscience.wiley.com.]

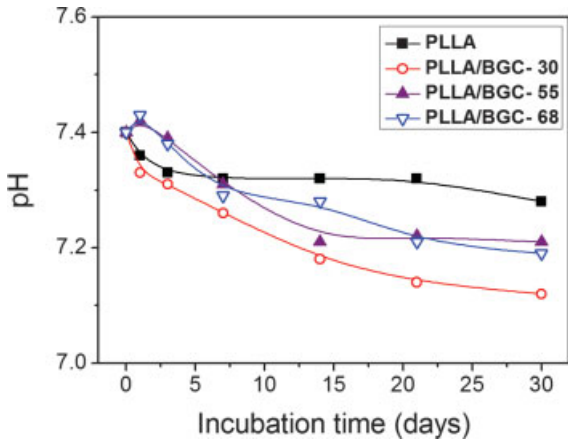

Figure 9. Change in pH in PBS medium versus incubation time for the porous scaffold of PLLA and the different types of PLLA/BGC composites. [Color figure can be viewed in the online issue, which is available at www.interscience.wiley.com.]

decrease of the porosity after introduction of inorganic filler in the polymeric fraction.[40] After 7 days of incubation, water absorption reached a maximum and stabilized at that value until 30 days of incubation time for all samples. No significant difference could be seen in the trends among the three types of PLLA/BGC composites.

The pH variation of the media containing different types of PLLA/BGC composites was presented in Figure 9. A burst decrease in pH value occurred at early incubation time for PLLA and PLLA/BGC-30 composite. The pH value for PLLA and PLLA/BGC-30 were always lower than the initial value during the entire incubation time range. After 3 days of incubation, the pH value of the medium for neat PLLA foam reached a plateau value at around 7.3, whereas the pH value for PLLA/BGC-30 continuously decreased during the 30 days of incubation time. For the case of both PLLA/BGC-55 and PLLA/BGC-68 composites, the pH value of the incubation medium slightly increases in the first day of incubation and then decreased gradually, stabilizing at around 7.2 after 2 weeks of incubation time. Degradation of PLLA releases a lot of acidic low molecular weight products that could rapidly decrease the pH value of incubation medium. Meanwhile, Ca and Si ions dissolved from BGC particles can compensate the decrease of pH value due to the acidic products of PLLA degradation. This neutralization effect of basic ions released from BGC particles could provide a pH buffering effect on the material surface contacted with PBS.[11,41] Comparing with BGC-55 and BGC-68, BGC-30 did not exhibit a notable compensation effect on the pH value of incubation medium, which was very similar to the result of incorporation of HAP particle into PLA matrix.[41]

The weight loss for the porous PLLA and PLLA/BGC composite scaffolds were shown in Figure 10. There was a rapid increase in weight loss for all composites independently on the BGC composition for early incubation times, followed by a more slow variation of this quantity. Compared with composite scaffolds, pure PLLA foam demonstrated a slow weight loss rate. During the 30 days of incubation period, the PLLA scaffold just lost about 2 wt % of its initial mass; such mass loss was consistent with the typical degradation profile of PLLA that may be considered as a slow biodegradable polymer. The weight loss for PLLA/BGC-30 composite was slightly higher than the other two composites. After 30 days of incubation the PLLA/BGC-30 composites could have lost about 6% of the initial mass, whereas the weight loss for the PLLA/BGC-55 and PLLA/BGC-68 were in range of 4–5%. Weight loss of composites resulted from not only the degradation of PLLA but also dissolution of BGC particles during incubation in PBS. Degradation of PLLA first occurred on the interface that was contacted with PBS. Introduction of hydrophilic BGC particles could absorb PBS into the inside of composite so that the interface between PLLA matrix and PBS would be increased. No doubt, it would accelerate the degradation of PLLA matrix. Compared with BGC-55 and BGC-68, BGC-30 showed a more accelerative effect on the degradation of PLLA matrix. This should be attributed to the low dissolubility of crystallized BGC-30 particle in PBS. The *in vitro* degradation results suggest that BGC-55 and BGC-68, when compared with BGC-30, might delay the degradation of the composite scaffolds by the neutralization effect of alkaline ions that were released from the BGC nanoparticles in the PBS medium. In a tissue engi-

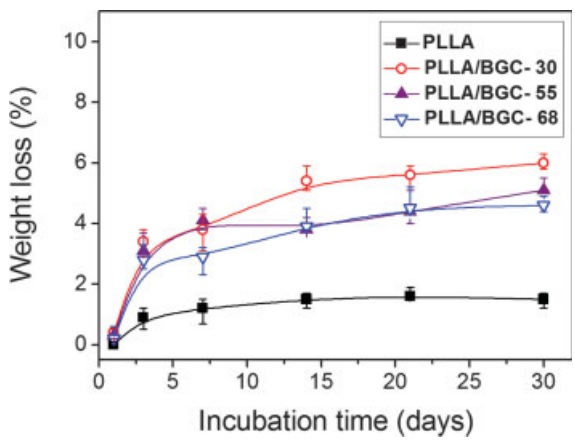

Figure 10. Weight loss versus incubation time in PBS for the porous scaffold of PLLA and the different types of PLLA/BGC composites. [Color figure can be viewed in the online issue, which is available at www.interscience.wiley.com.]

neering context, this could have a beneficial effect at a longer implantation time scale, avoiding the typical consequences resulting from the decrease of pH due to polymer hydrolysis.

CONCLUSIONS

Different formulations of BGC nanoparticles were obtained by a three-step sol–gel method in the presence of PEG as surfactant. This method enabled to obtain particles with sizes of around 20 nm. The XRD patterns for the different types of BGC nanoparticles showed that for higher contents of phosphate the SiO_2-P_2O_5-CaO glass ceramic system could exhibit a crystalline structure upon calcification at 700°C. Hence, the BGC particles with lower phosphate content demonstrated higher solubility in PBS medium when compared with BGC-30. The porous scaffolds of PLLA/BGC composites were prepared by a thermal induced phase separation method. The microstructure of the PLLA/BGC composite foams consisted of pores with 10–300 μm diameter separated by 2–5 μm thick walls. In addition, the *in vitro* tests indicated that BGC-55 and BGC-68 have better bioactivity than BGC-30. These results suggest that these novel BGC nanoparticles may find applications in the development of new systems for bone tissue engineering and bone tissue regeneration.

The authors acknowledge Dr. Aixue Liu for the ESEM, XRD, and FTIR testing at Changchun Institute of Applied Chemistry.

References

1. Hench LL, Splinter RJ, Allen WC. Bonding mechanisms at the interface of ceramic prosthetic materials. J Biomed Mater Res Symp 1971;2:117–141.
2. Hench LL, Wilson J. Surface-active biomaterials. Science 1984;226:630–636.
3. Xynos ID, Hukkanen MVJ, Buttery LDK, Hench LL, Polak JM. Bioglasss 45S5 stimulates osteoblast turnover and enhances bone formation *in vitro*: Implications and applications for bone tissue engineering. Calcif Tissue Int 2000;67:321–329.
4. Hench LL, Paschall HA. Direct chemical bond of bioactive glass-ceramic materials to bone and muscle. J Biomed Mater Res 1973;7:25–42.
5. Wheeler DL, Montfort MJ, McLoughlin SW. Differential healing response of bone adjacent to porous implants coated with hydroxyapatite and 45S5 bioactive glass. J Biomed Mater Res A 2001;55:603–612.
6. Jones JR, Hench LL. Biomedical materials for new millennium: Perspective on the future. Mater Sci Technol 2001;17: 891–900.
7. Li N, Jie Q, Zhu S, Wang R. A new route to prepare macroporous bioactive sol-gel glasses with high mechanical strength. Mater Lett 2004;58:2747–2750.
8. Jones JR, Ehrenfried LM, Hench LL. Optimising bioactive glass scaffolds for bone tissue engineering. Biomaterials 2006; 27:964–973.
9. Roman J, Padilla S, Vallet-Regí M. Sol-gel glasses as precursors of bioactive glass ceramics. Chem Mater 2003;15:798–806.
10. Vallet-Regí M, Rámila A. New bioactive glass and changes in porosity during the growth of a carbonate hydroxyapatite layer on glass surfaces. Chem Mater 2000;12:961–965.
11. Boccaccini AR, Maquet V. Bioresorbable and bioactive polymer/Bioglass® composites with tailored pore structure for tissue engineering applications. Compos Sci Technol 2003;63: 2417–2429.
12. Ramakrishna S, Mayer J, Wintermantel E, Leong KW. Biomedical applications of polymer-composite materials: A review. Compos Sci Technol 2001;61:1189–1224.
13. Chim H, Hutmacher DW, Chou AM, Oliveira AL, Reis RL, Lim TC, Schantz J-T. A comparative analysis of scaffold material modifications for load-bearing applications in bone tissue engineering. Int J Oral Max Surg 2006;35:928–934.
14. Leonor IB, Sousa RA, Cunha AM, Reis RL, Zhong ZP, Greenspan D. Novel starch thermoplastic/Bioglass® composites: Mechanical properties, degradation behavior and *in-vitro* bioactivity. J Mater Sci: Mater Med 2002;13:939–945.
15. Korventausta J, Jokinen M, Rosling A, Peltola T, Yli-Urpo A. Calcium phosphate formation and ion dissolution rates from silica gel-PDLLA composites. Biomaterials 2003;24:5173–5178.
16. Boccaccini AR, Blaker JJ, Maquet V, Chung W, Jerome R, Nazhat SN. Poly(D,L-lactide) PDLLA foams with TiO_2 nanoparticles and PDLLA/TiO_2-bioglass foam composites for tissue engineering scaffolds. J Mater Sci 2006;41:3999–4008.
17. Blaker JJ, Maquet V, Jerome R, Boccaccini AR, SN Nazhat. Mechanically anisotropic PDLLA/Bioglass composite foams as scaffolds for bone tissue engineering. Acta Biomater 2005; 1:643–652.
18. Maquet V, Boccaccini AR, Pravata L, Notingher I, Jérôme R. Preparation, characterization, and *in vitro* degradation of bioresorbable and bioactive composites based on bioglass-filled polylactide foams. J Biomed Mater Res A 2003;66:335–346.
19. Blaker JJ, Gough JE, Maquet V, Notingher I, Boccaccini AR. *In vitro* evaluation of novel bioactive composites based on Bioglass-filled polylactide foams for bone tissue engineering scaffolds. J Biomed Mater Res A 2003;67:1401–1411.
20. Roether JA, Boccaccini AR, Hench LL, Maquet V, Gautier S, Jérôme R. Development and *in vitro* characterisation of novel bioresorbable and bioactive composite materials based on polylactide foams and Bioglass(R) for tissue engineering applications. Biomaterials 2002;23:3871–3878.
21. Verrier S, Blaker JJ, Maquet V, Hench LL, Boccaccini AR. PDLLA/Bioglass(R) composites for soft-tissue and hard-tissue engineering: An *in vitro* cell biology assessment. Biomaterials 2004;25:3013–3021.
22. Day RM, Maquet V, Boccaccini AR, Jérôme R, Forbes A. *In vitro* and *in vivo* analysis of macroporous biodegradable poly(D,L-lactide-*co*-glycolide) scaffolds containing bioactive glass. J Biomed Mater Res A 2005;75:778–787.
23. Clark AE, Hench LL. Calcium phosphate formation on sol-gel derived bioactive glasses. J Biomed Mater Res 1994;28:693–698.
24. Hench LL. Sol-gel materials for bioceramic applications. Curr Opin Solid State Mater Sci 1997;2:604–610.
25. Rezwan K, Chen Q, Blaker JJ, Boccaccini AR. Biodegradable and bioactive porous polymer/inorganic composite scaffolds for bone tissue engineering. Biomaterials 2006;27:3413–3431.
26. Kothapalli CR, Shaw MT, Wei M. Biodegradable HA-PLA 3-D porous scaffolds: Effect of nano-sized filler content on scaffold properties. Acta Biomater 2005;1:653–662.
27. Roco MC. Nanoparticles and nanotechnology research. J Nanoparticle Res 1999;1:1–6.
28. Hong Z, Zhang P, Liu A, Chen L, Chen X, Jing X. Composites of poly(lactide-*co*-glycolide) and the surface modified carbonated hydroxyapatite nanoparticles. J Biomed Mater Res A 2007;81:515–522.

29. Hong Z, Zhang P, He C, Qiu X, Liu A, Chen L, Chen X, Jing X. Nano-composite of poly(L-lactide) and surface grafted hydroxyapatite: Mechanical properties and biocompatibility. Biomaterials 2005;26:6296–6304.
30. Runner TB, Grass R, Stark W. Glass and bioglass nanopowders by flame synthesis. Chem Commun 2006;13:1384–1386.
31. Shchipunov YA, Karpenko TY, Bakunina IY, Burtseva YV, Zvyagintseva TN. A new precursor for the immobilization of enzymes inside sol-gel-derived hybrid silica nanocomposites containing polysaccharides. J Biochem Biophys Methods 2004;58:25–38.
32. Yokoyama R, Suzuki S, Shirai K, Yamauchi T, Tsubokawa N, Tsuchimochi M. Preparation and properties of biocompatible polymer-grafted silica nanoparticle. Eur Polym J 2006; 42:3221–3229.
33. Cheng W, Wang Z, Ren C, Chen H, Tang T. Preparation of silica/polyacrylamide/polyethylene nanocomposite via *in situ* polymerization. Mater Lett 2007;61:3193–3196.
34. Hong Z, Liu A, Zhuang X, Chen L, Chen X, Jing X. Preparation of bioactive ceramic nanoparticles by a novel method. Submitted for publication.
35. Maquet V, Boccaccini AR, Pravata L, Notingher I, Jérôme R. Porous poly(α-hydroxyacid)/Bioglasss composite scaffolds for bone tissue engineering. I. Preparation and *in vitro* characterization. Biomaterials 2004;25:4185–4194.
36. Kokubo T, Takadama H. How useful is SBF in predicting *in vivo* bone bioactivity? Biomaterials 2006;27:2907–2915.
37. Boesel LF, Cachinho SCP, Fernandes MHV, Reis RL. The *in vitro* bioactivity of two novel hydrophilic, partially degradable bone cements. Acta Biomater 2007;3:175–182.
38. Peitl O, LaTorre GP, Hench LL. Effect of crystallization on apatite layer formation of bioactive glass 45S5. J Biomed Mater Res 1996;30:509–514.
39. Li P, Zhang F, Kokubo T. The effect of residual glassy phase in a bioactive glass-ceramic on the formation of its surface apatite layer *in vitro*. J Mater Sci: Mater Med 1992;3:452–456.
40. Cao W, Hench LL. Bioactive ceramics. Ceram Int 1995;22: 493–507.
41. Li H, Chang J. pH-compensation effect of bioactive inorganic fillers on the degradation of PLGA. Compos Sci Technol 2005;65:2226–2232.